Geomagnetically-induced effects related to disturbed geomagnetic field variations at low latitude

N Kouassi* , V Doumbia, K Boka, Z Tuo, O D F Grodji, A A Kassamba and A F Zillé

Laboratoire de Physique de l'Atmosphère, UFR-SSMT, Université Félix Houphouët Boigny, Abidjan, Côte d'Ivoire.
*Corresponding author. e-mail: nguessank23@yahoo.fr

In this paper, we analyzed low latitude geoelectric field variations and Geomagnetically Induced Current (*GIC*), associated with disturbed geomagnetic field variations in West Africa. For this purpose, variations of geomagnetic field components H, D and Z, and geoelectric field horizontal components Ey and Ex were examined during geomagnetically disturbed periods, with the daily means of the Ap index higher than 20 nT. Variations of geoelectric field components Ey and Ex were identified as associated with disturbed variations of the geomagnetic field. The *GIC* was estimated from the observed Ey and Ex based on system parameters configuration with $a = b = 50\,\mathrm{A\,km/V}$. The disturbance fluctuations in the geoelectric field components and the estimated *GIC* exhibit a diurnal trend, with higher amplitudes during the daytime. The impulses in the geoelectric field components and the estimated *GIC* are stronger in the southern stations than in the northern stations. On the average, these impulses decrease from LAM to TOM, with a slight enhancement near the magnetic equator.

Keywords. Geomagnetic field impulsive variations; geoelectric field; geomagnetically induced currents; low latitudes.

1. Introduction

The Sun continuously blows ionized particles known as 'solar wind' in the interplanetary space. Following intense coronal mass ejection (CME), the compression of the magnetosphere by the solar wind and the interaction with the geomagnetic field intensify currents in the magnetosphere and high latitude ionosphere (Bogdan 2007). The subsequent intense fluctuations of the geomagnetic field during the disturbance periods (geomagnetic storms) induce electric field and currents within the earth (Boteler *et al.* 1998; Pirjola 2000; Pirjola *et al.* 2005). These currents are designated as 'geomagnetically induced currents (GIC)'. The flows of GIC in technological infrastructures, such as buried pipelines, power

transmission system, transformers and telecommunication cables, are known to possibly cause their disruption. Such damages have been experienced at high latitudes since mid XIXth century (Bolduc 2002; Boteler 2001). The disruptions of Hydro–Quebec (Canada) power grid on March 13th, 1989, which resulted in a 9-h power outage (Boteler *et al.* 1998) and that in Sweden on October 30th, 2003, are noticeable GIC effects that occurred in the modern days (Kappenman 2005). At high latitudes, magnetosphere–ionosphere coupling through geomagnetic field lines generates intense currents such as auroral electrojets (Viljanen and Pirjola 1994; Pulkkinen *et al.* 2003). These currents are extremely enhanced during geomagnetic storms and substorms and cause very intense geomagnetic field

variations. Thus, most investigations on GICs have been focused on high latitudes (Bolduc 2002; Lam *et al.* 2002; Pirjola 2005; Pulkkinen *et al.* 2005; Wik *et al.* 2009). There are only few reports on important *GIC* occurrence in low- and mid-latitudes (Trivedi *et al.* 2007; Ngwira *et al.* 2008, 2015; Torta *et al.* 2012). However, several transformer failures due to GIC associated with geomagnetic storms occurred in South Africa between 2003 and 2004 (Gaunt and Coetzee 2007). Trivedi *et al.* (2007) estimated the *GIC* amplitudes during the November 7–10, 2004 geomagnetic storm in Brazil. They obtained *GIC* values between 15 and 20 A. Impulsive variations of the geomagnetic field like sudden storm commencement (ssc) and solar flare effects (sfe) are the possible sources of significant GICs at low latitudes (de Villiers *et al.* 2016; Kappenman 2003, 2005). In a recent study, Doumbia *et al.* (2017) analyzed the low latitude geoelectric field variations observed in West Africa in 1993. In that study, enhanced geoelectric field variations have been associated with impulsive geomagnetic field variations like *sscs* and *sfes*. However, the GICs associated with those variations have not been estimated.

It is worth to notice that GIC estimations in most previous studies are inferred from geomagnetic field variations (Koen 2000; Bernhardi *et al.* 2008, 2010; Liu *et al.* 2009; Barbosa *et al.* 2015). The approach consists of estimating the horizontal components (*Ey* and *Ex*) of the geoelectric field variations from the time derivatives of the geomagnetic field variations based on a given earth conductivity model. The resulting geoelectric field components are then used to calculate the GIC. This approach assumes the local earth's conductivities are known before.

In the present work, the disturbed geomagnetic field variations and associated geoelectric field variations observed at different stations in West Africa are analyzed. In addition, variations of the GIC was estimated from the respective measured geoelectric field components *Ey* and *Ex*.

2. Data and data processing

2.1 *Data*

During the International Equatorial Electrojet Year (IEEY), 10 stations devoted to recording the geomagnetic and geoelectric field variations were deployed along a meridian chain across the geomagnetic dip-equator in West Africa

(Amory-Mazaudier *et al.* 1993; Doumouya *et al.* 1998; Vassal *et al.* 1998; Doumbia *et al.* 2017). The stations were located along the 5°W meridian, from Lamto (Cote d'Ivoire, –6.30° dip-latitudes) to Tombouctou (Mali, +6.76° dip-latitudes). Figure 1 shows the IEEY network of the stations in West Africa. The coordinates of the stations are given in table 1. Variations of the horizontal northward (*H*), eastward (*D*) and vertical (*Z*) components of the geomagnetic field, as well as the north–south (*Ex*) and east–west (*Ey*) components of the geoelectric field were recorded at a sampling rate of 1 min from November 1992 to December 1994. The *H* and *D* components were measured with suspended magnet variometers with an accuracy of about ± 0.2 nT and thermal sensitivity of 0.02 nT/°C. The *Z* component was recorded with a fluxgate magnetometer with an accuracy of ± 0.1 nT. Geoelectric field variations were measured as potential differences between electrodes installed at the ends of two 200 m long lines oriented along N–S and E–W magnetic directions, respectively. The measured potential differences resulted from the circulation of the geoelectric field between the two ends of the line, and were therefore proportional to the average value of the geoelectric component along the line (*Ex* for the N–S line and *Ey* for the E–W line, respectively). Each electrode was made from five thin sheets of lead metal (20 cm × 10 cm) buried at a depth of 50 cm. The measured geoelectric signal was amplified, with the resultant output being in the range of ± 250 mV/km with 0.13 mV/km sensitivity. *In-situ* measurements showed that differential variations of temperature between two electrodes set 50 cm deep were about 0.2°C for a daily temperature variation of about 15°C at the surface, thereby resulting in a negligible thermal drift of 5–10 μV (Vassal *et al.* 1998). The schematic diagram of the measurement is shown in figure 2.

2.2 *Data processing*

2.2.1 *Geoelectric field data*

The total geoelectric field component Ex_{tot} measured in each station can be expressed by:

$$Ex_{tot}(t) = Ex(t) + Ex_{bl}(t) \qquad (1)$$

where *Ex* is the geoelectric field fluctuations that are superimposed on the geoelectric field diurnal variation Ex_{bl}. Ex_{bl} was removed by polynomial fitting of degree 16. The degree 16 is chosen after
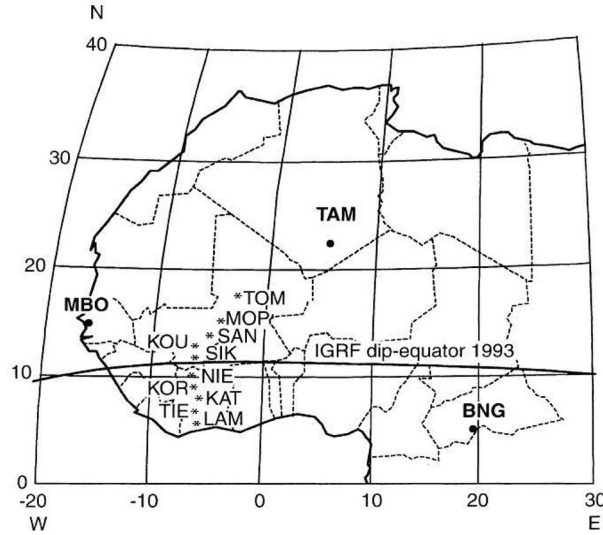
Figure 1. The West African network of 10 stations for the geomagnetic and geoelectric field measurements during the International Equatorial Electrojet Year (IEEY).

Table 1. *Geographic coordinates of the magnetic stations installed along the meridian 5°W in West Africa during the International Equatorial Electrojet Year. The geomagnetic dip-latitudes of the stations at epoch 1993.5 are shown.*

Stations	Station codes	Latitude (°N)	Longitude (°W)	Dip-latitude (°N)
Tombouctou	TOM	16.733	3.000	6.76
Mopti	MOP	14.508	4.087	4.02
San	SAN	13.237	4.879	2.45
Koutiala	KOU	12.356	5.448	1.38
Sikasso	SIK	11.344	5.706	0.12
Nielle	NIE	10.203	5.636	−1.30
Korhogo	KOR	9.336	5.427	−1.88
Katiola	KAT	8.183	5.044	−3.85
Tiébissou	TIE	7.218	5.241	−5.04
Lamto	LAM	6.233	5.017	−6.30

many iterations from 0 to 50. Ex is obtained by substracting the base line Ex_{bl} from Ex_{tot}:

$$Ex(t) = Ex_{tot}(t) - Ex_{bl}(t). \quad (2)$$

Similar calculation is made for Ey component.

2.2.2 *Geomagnetically induced current calculation methods*

The geomagnetically induced current in any technological system can be calculated by the following equation:

$$GIC(t) = aEx(t) + bEy(t) \quad (3)$$

where Ex and Ey are the fluctuations of the horizontal geoelectric filed components, and a and b are designated as system parameters. a and b depend on the topology and the electrical characteristics of the system concerned. In practice, a and b can be determined if GIC and the geoelectric field or GIC and the geomagnetic field variations are known. When the values of the geoelectric field components and the GIC are known, a and b can be estimated as follows (Pulkkinen *et al.* 2007; Ngwira *et al.* 2008):

$$a = \frac{\langle GICE_y \rangle \langle E_x E_y \rangle - \langle GICE_x \rangle \langle E_y^2 \rangle}{\langle E_x E_y \rangle^2 - \langle E_x^2 \rangle \langle E_y^2 \rangle} \quad (4)$$

$$b = \frac{\langle GICE_x \rangle \langle E_x E_y \rangle - \langle GICE_y \rangle \langle E_x^2 \rangle}{\langle E_x E_y \rangle^2 - \langle E_x^2 \rangle \langle E_y^2 \rangle} \quad (5)$$
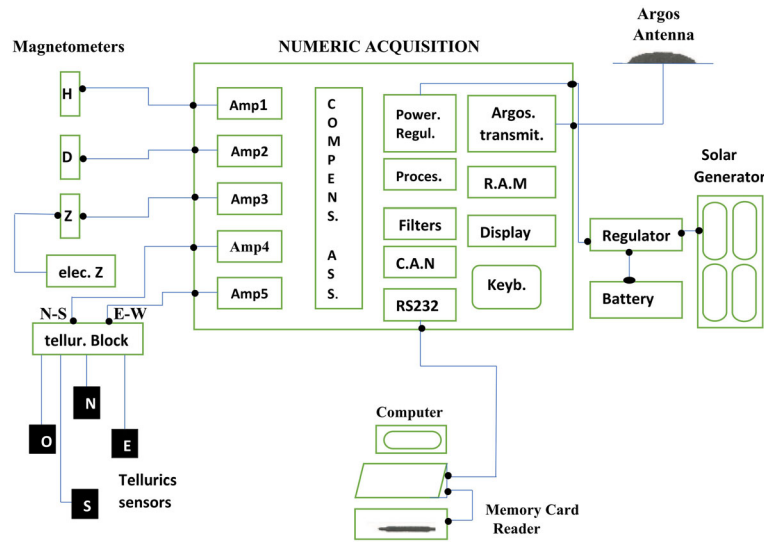
Figure 2. Synoptic scheme of a geomagnetic-telluric station used to measure the variations of the east–west D (channel 1), horizontal H (channel 2), and vertical Z (channel 5) components of the geomagnetic B field and the north–south (NS) (channel 3) and east–west (EW) (channel 4) components of the telluric B field (Doumouya 1995).

Table 2. *Tri-hourly ap index and the daily mean Ap index for the selected days.*

Dates	Tri-hourly ap index (nT)								Ap (nT)
1993-01-10	18	27	80	27	27	15	4	4	25
1993-01-31	32	56	80	67	48	39	67	80	59
1993-02-17	7	27	22	39	111	67	9	5	36
1993-02-20	15	27	39	32	22	12	15	48	26
1993-03-09	111	111	94	67	39	32	18	39	64
1993-03-11	12	5	15	39	67	111	80	67	50
1993-03-15	32	22	67	56	56	39	32	56	45
1993-03-16	32	48	56	39	12	67	48	9	39
1993-03-24	27	80	154	80	39	32	18	32	58
1993-04-04	6	6	4	5	48	80	132	179	58
1993-04-05	94	154	132	67	94	67	67	18	87

where a and b are expressed in A. km/V and the symbol '.' indicates the expectation values of the parameters.

3. Results

3.1 *Geomagnetic and geoelectric field variations during quiet periods*

In this section, quiet period geomagnetic and geoelectric field data are analyzed. H, D and Z components on 23 February, 1993 with Ap = 9 nT are shown in figure 3. Figure 4(a and b) shows variations of the total geoelectric field, the baseline and the fluctuations on 23 February, 1993. The baseline shows a high variability from one station to another. The amplitudes of the fluctuations are weak, including at LAM where it appears to have strong amplitude. The storm effects on Ex and Ey, are shown on the composite hourly mean and the standard deviation of these components during quiet and disturbed periods in figure 5(a and b). It appears that the amplitudes of the standard deviation of the fluctuations Ex and Ey are higher during storm periods than on quiet days. Ex and Ey data are far away from the mean value during the disturbed period than during a quiet period.

3.2 *Geomagnetic and geoelectric field variations during disturbed periods*

In the present study, geomagnetic field and geoelectric field variations during 11 disturbed days with the daily Ap index higher than 20 nT are
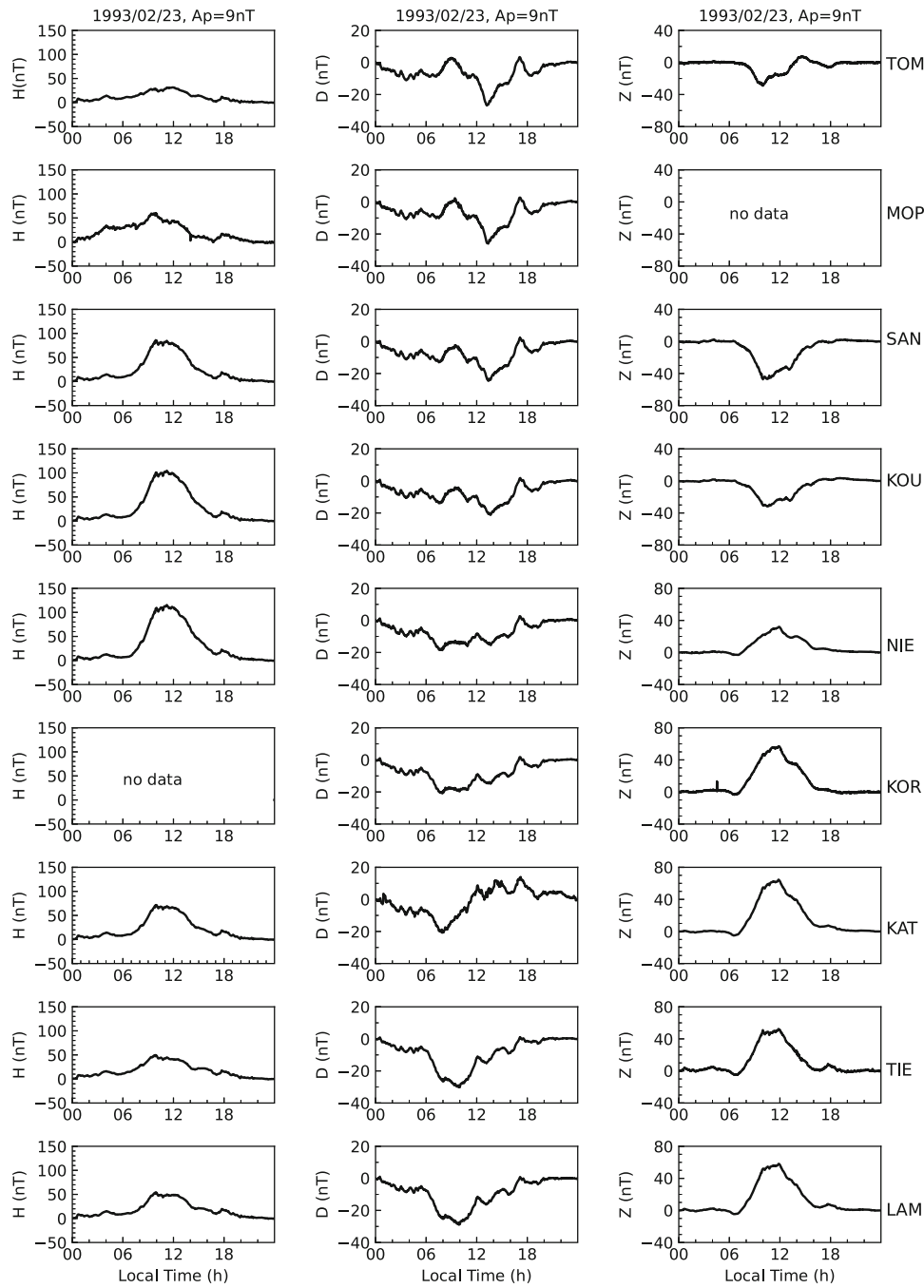
Figure 3. The geomagnetic components H, D and Z at West African stations during the quiet day of 23 February, 1993. The Ap value (9 nT) of this day is shown.

considered. The tri-hourly ap indices and the daily Ap index shown in table 2 were downloaded from http://swdcwww.kugi.kyoto-u.ac.jp/index.html.

Figure 6 shows variations of the H (a), D (b) and Z (c) components of the geomagnetic field, the time derivatives dH/dt (d), dD/dt (e) and dZ/dt (f) and the fluctuations of the geoelectric field components Ex (g) and Ey (h) observed at LAM, respectively on 10 January 1993 (left column), on 20 February,

1993 (middle column) and 15 March, 1993 (right column). The geoelectric field fluctuations were isolated from the daily variations of Ex and Ey according to the method described in equation (2). On the three days shown in figure 6, the daily Ap indices are respectively 25, 26, 45 nT with 80, 39 and 67 nT as highest values of tri-hourly *ap*. The high values of the *ap* indices indicate significant geomagnetic field disturbances, which are
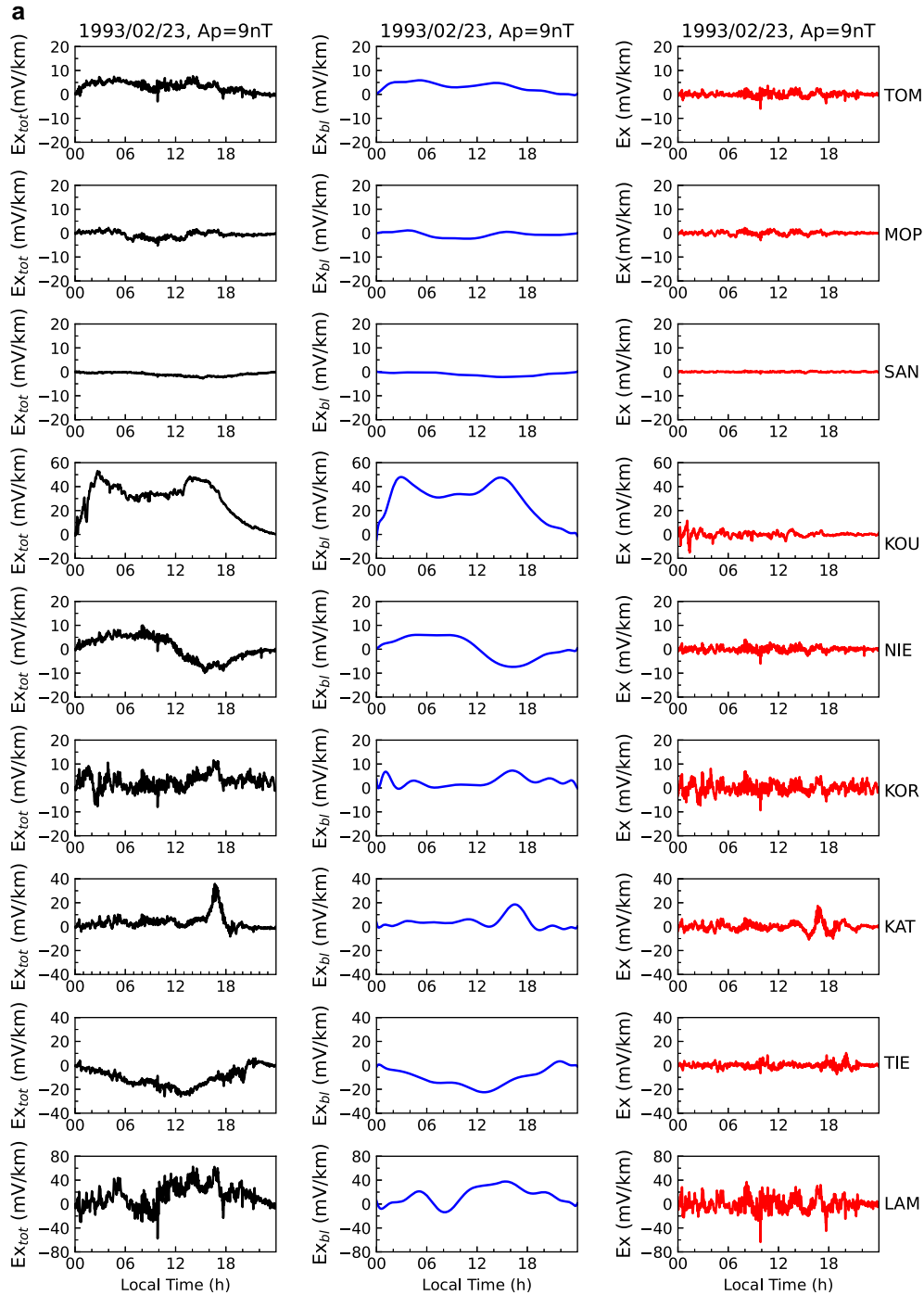
Figure 4. (**a**) The daily geoelectric field Ex_{tot} (left column), the isolated baseline Ex_{bl} (middle column) and the fluctuations Ex (right column) on 23 February, 1993. (**b**) The daily geoelectric field Ey_{tot} (left column), the isolated baseline Ey_{bl} (middle column) and the fluctuations Ey (right column) on 23 February, 1993.

confirmed by the geomagnetic field components H, D and Z and their time derivative dH/dt, dD/dt and dZ/dt that exhibit important fluctuations. As a consequence, significant variations of the geoelectric field components Ex and Ey, associated with these fluctuations are observed. Indeed, variations of Ex and Ey clearly reflect respectively the

fluctuations of the time derivatives dD/dt and dH/dt of the geomagnetic field components. The correlation between Ex and dD/dt, and Ey and dH/dt is shown in figure 7. The correlation coefficient between Ey and dH/dt is about -0.87 during the three storms, while that of Ex and dD/dt is greater than or equal to 0.60.
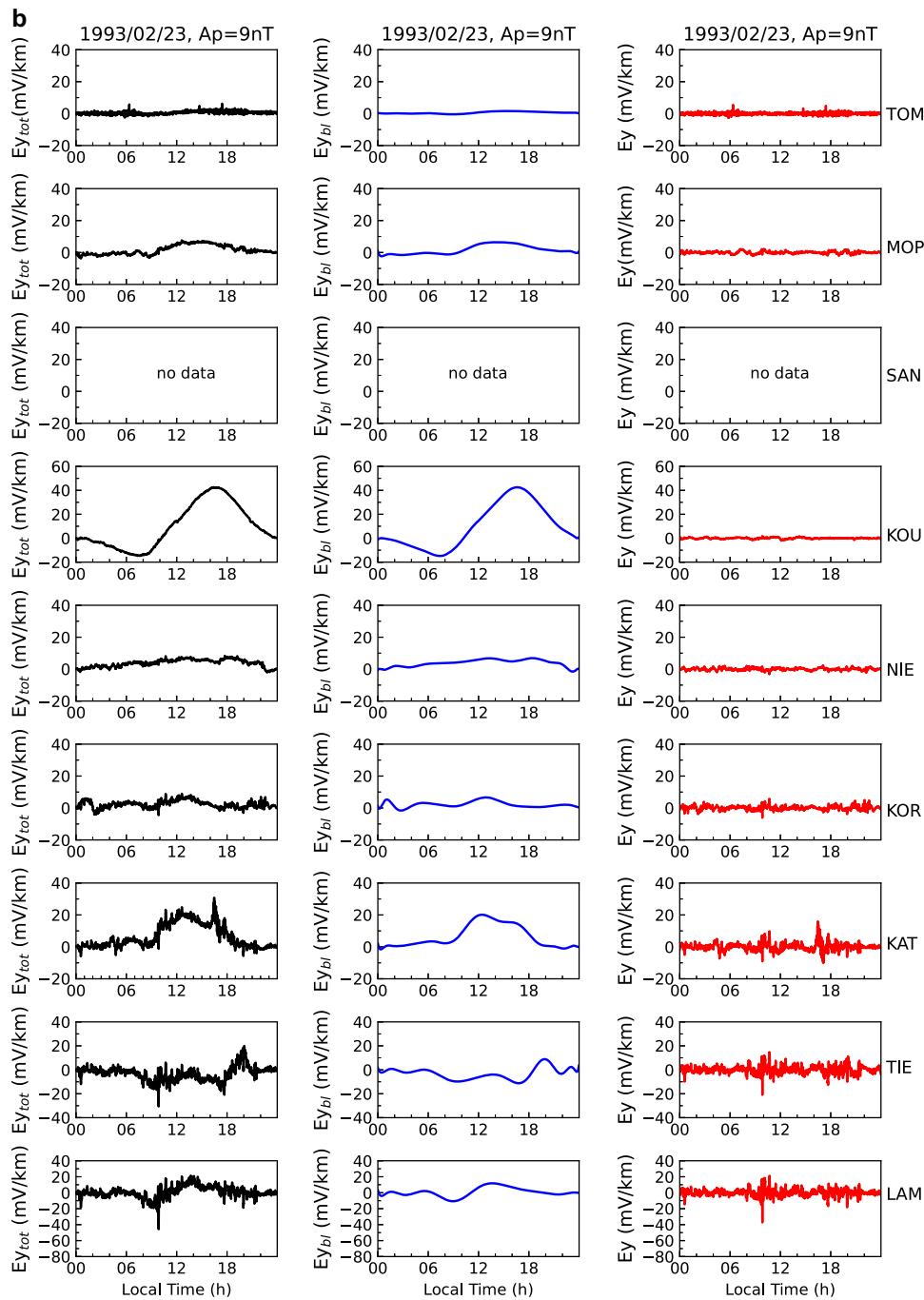
Figure 4. (*Continued.*)

3.3 *Induction effects associated with disturbed fluctuations of the geomagnetic field*

3.3.1 *Geoelectric field variations associated with disturbed geomagnetic fluctuations*

In this section, variations of the geoelectric field horizontal components Ex and Ey, recorded during 11 geomagnetically disturbed days (table 2), are analyzed. Figure 8(a and b) shows fluctuations of the geoelectric field components Ex and Ey associated with geomagnetic disturbances on 10 January and 15 March, 1993 (first two columns on the left), and 20 February and 24 March, 1993 (last two columns on the right), at different stations of the network. For these disturbed days, the geoelectric field components exhibit rapid fluctuations that were isolated from the measured geoelectric field components, by subtracting the baseline (Doumbia *et al.* 2017).
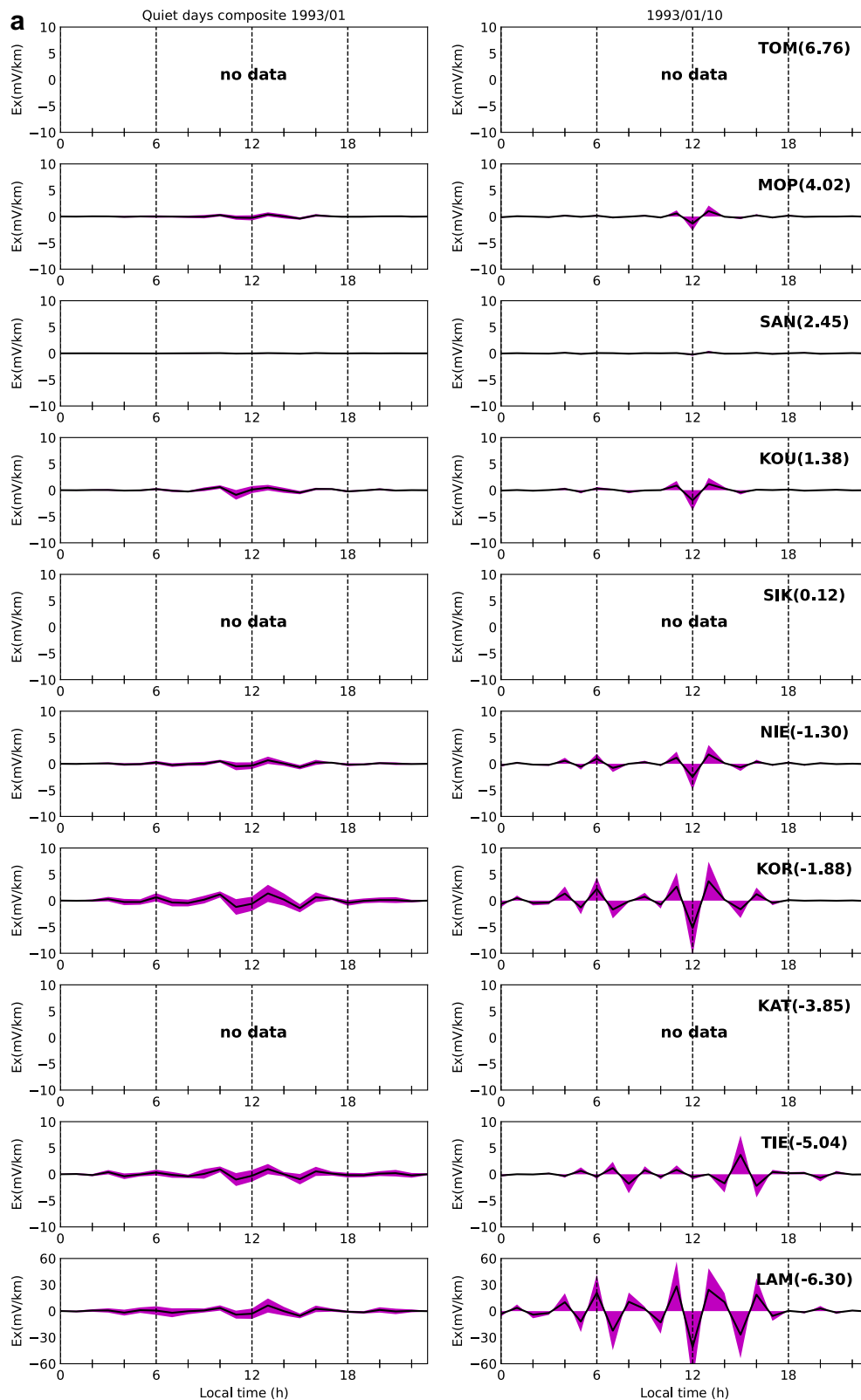
Figure 5. (**a**) The *Ex* composite hourly mean and standard deviation estimated with five quiet days in January, 1993 and that of the disturbed day of January 10, 1993. In each panel of the figure, the name and the dip latitude value of the station are indicated. (**b**) Same as figure 5(a), but for *Ey*.

These fluctuations associated with geomagnetic variations are observed at all the stations of the network. The magnitudes of the fluctuations show a diurnal trend with most significant amplitudes observed during the daytime. In addition, strong impulses due to brisk changes in the magnetic field
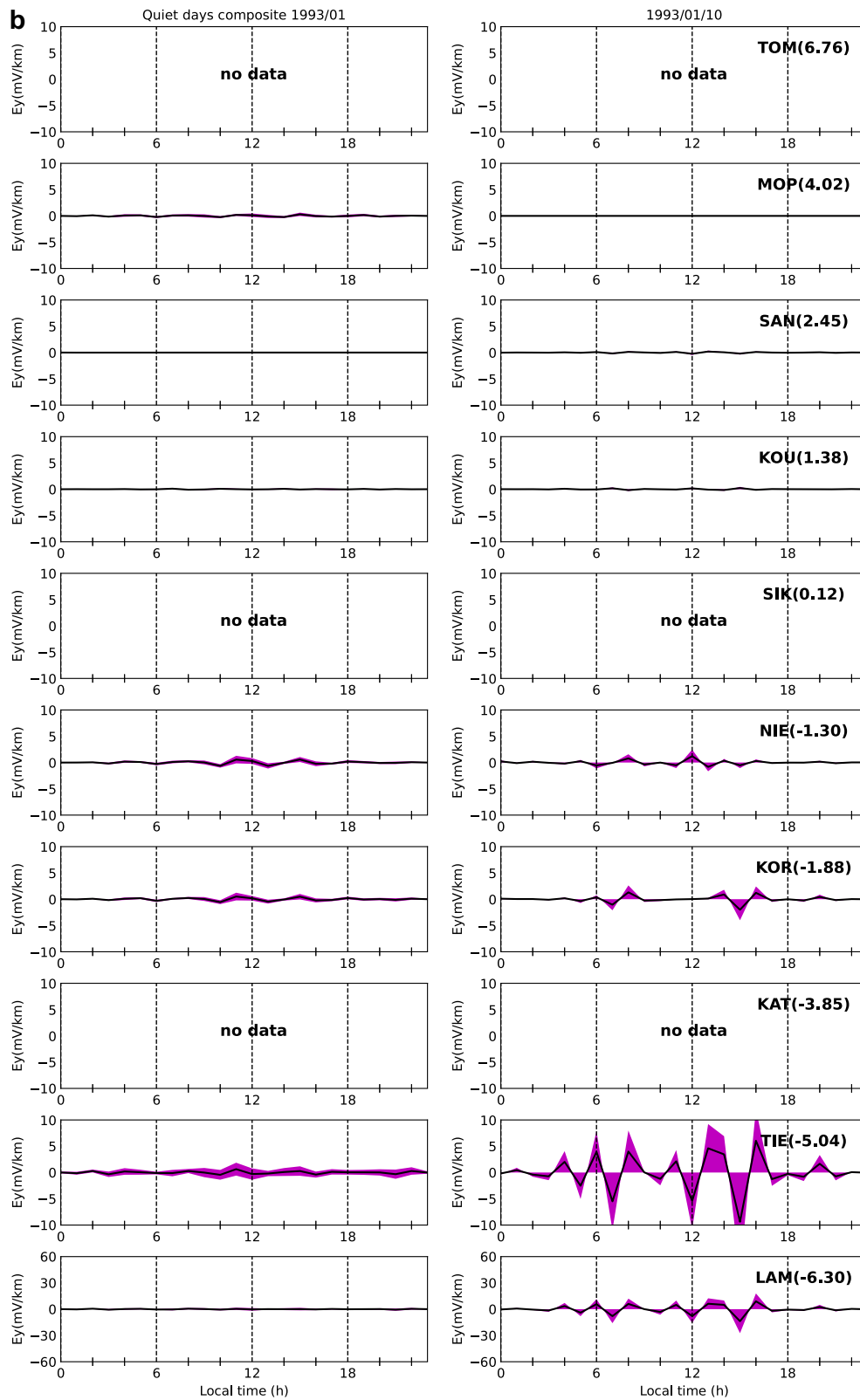
Figure 5. (*Continued.*)

variations are observed. More attention is paid to these impulses in this study. On 10 January, 1993, the crest-to-crest amplitudes of the strongest impulse at LAM are $Ex = 369\,\text{mV/km}$ and $Ey = 289\,\text{mV/km}$ around 11.00 LT. On 20 February, 1993, $Ex = 352\,\text{mV/km}$ and $Ey = 186\,\text{mV/km}$
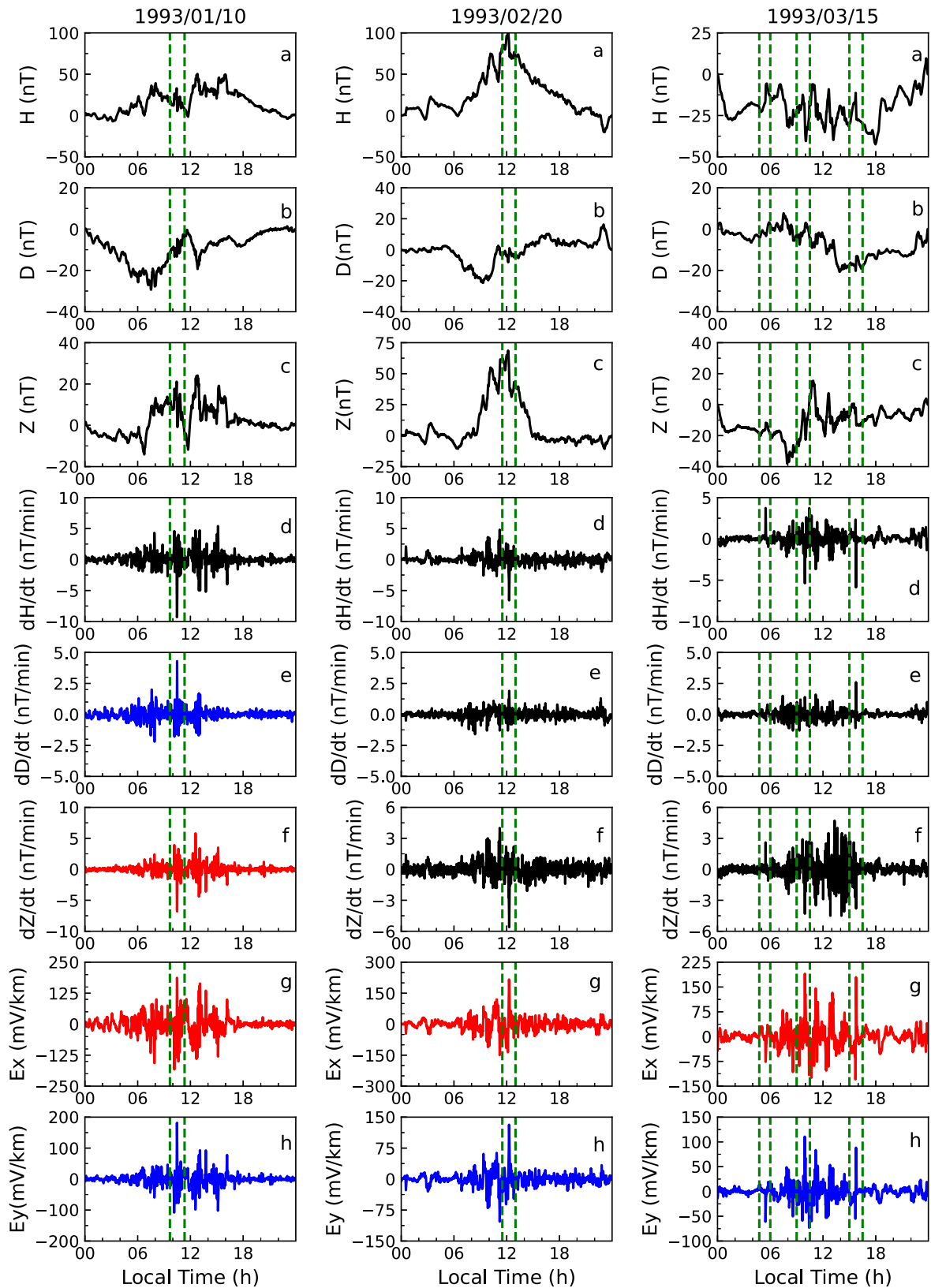
Figure 6. The geomagnetic field components H (**a**), D (**b**) and Z (**c**), the time derivatives dH/dt (**d**), dD/dt (**e**) and dZ/dt (**f**) and the geoelectric field components Ex (**g**) and Ey (**h**) recorded at LAM during three disturbed days: 10 January (left column), 20 February (middle column), and 15 March (right column), 1993.
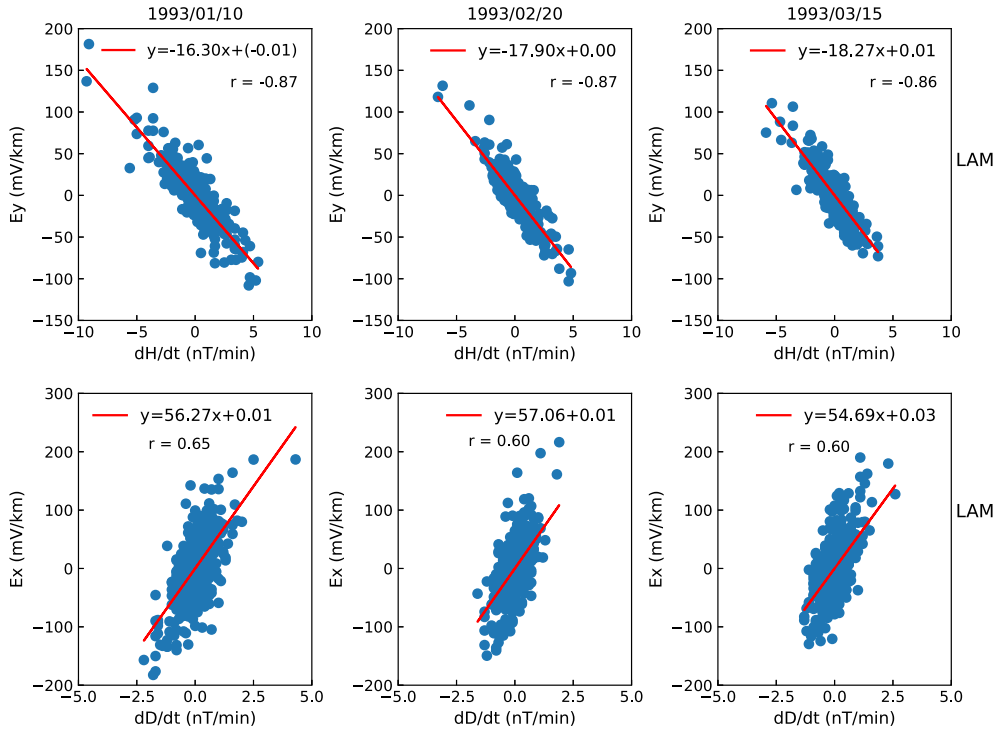
Figure 7. Correlations between *Ey* and *dH/dt*, and *Ex* and *dD/dt* at LAM during the disturbance periods of 10 January 1993, 20 February 1993 and 15 March 1993.

around 12.00 LT. The most important amplitudes of fluctuations and impulses are observed at LAM. However, they are also observed at all the stations. In section 3.2.3, the latitudinal trend of the impulses of the geoelectric field component are examined.

3.4 *Geomagnetically induced currents estimated from geoelectric field variations*

In this section, the geomagnetically induced current (GIC) within a ground-based network of conductors is estimated from the horizontal components *Ex* and *Ey* of geoelectric field variations, and *a* and *b* using the equation (3). Different values of *a* and *b* are found in literature (Liu *et al.* 2009; Pulkkinen *et al.* 2007, 2012; Matandirotya 2016). For example, Matandirotya *et al.* (2015) used $a = -94$ A. km/V and $b = 24$ A. km/V for the power grid in South Africa; Pulkkinen *et al.* (2007) used $a = -70$ A. km/V and $b = 88$ A. km/V for the Finnish natural gas pipeline and Liu *et al.* (2009) used $a = -3.5$ A. km/V and $b = -256$ A. km/V for the Chinese power grids. It is to be noticed that other values of *a* and *b* have also been used for the

GIC investigation (Bernhardi *et al.* 2008; Ngwira *et al.* 2008; Wik *et al.* 2009).

It is to be noticed that the system parameters *a* and *b* of the conductor systems are not determined during the IEEY campaign. For this study, the configuration of system parameters with $a = b = 50$ A. km/V is considered to estimate the GIC at different stations. This choice is based on the recommendation made by Pulkkinen *et al.* (2012), who demonstrated that a good approximation of the GIC is obtained when both *a* and *b* are set to 50 A. km/V for unknown conductor systems (Zois 2013). Same value of *a* and *b* can also be justified by the fact that during the IEEY campaign, the same electric wires of 200 m and electrodes were used in north–south and east–west directions for *Ex* and *Ey* measurements.

The GIC variations associated with the fluctuations of the geoelectric field components *Ex* and *Ey*, are estimated from equation (3), with more emphasis on the strong impulses. Figure 9(a and b) shows the estimated *GIC* variations on 10 January and 20 February 1993 (figure 9a), and 15 and 24 March, 1993 (figure 9b). Like that of geoelectric field components, the GIC variations exhibit a daily trend with higher magnitudes of the
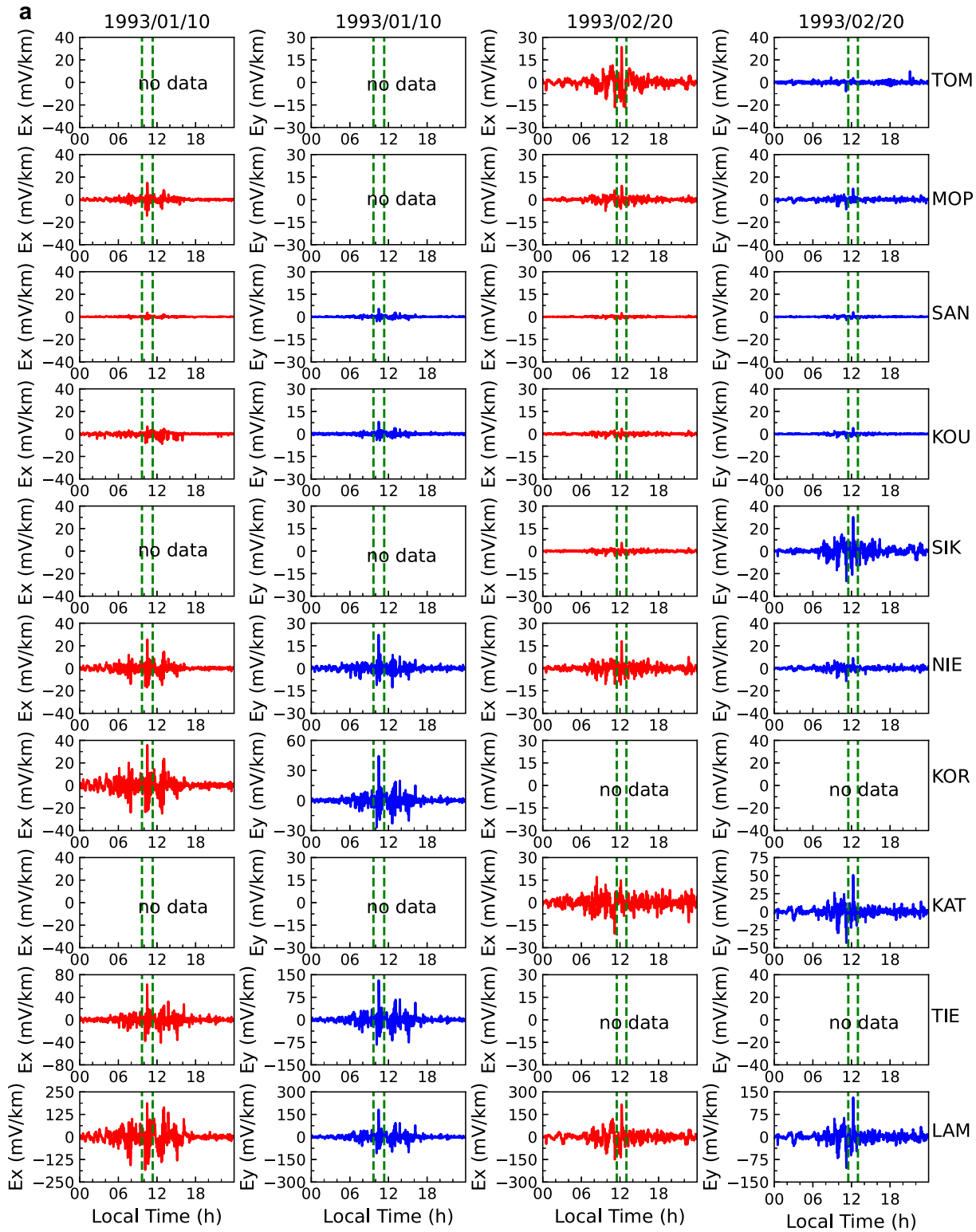
Figure 8. (**a**) Fluctuations of the geoelectric field components *Ey* and *Ex* associated with geomagnetic field disturbances on 10 January and 20 February, 1993. The vertical dashed lines indicate the selected impulses considered for the latitudinal variations of *Ey*, *Ex* and *GIC* in figure 10. (**b**) Same as figure 8(a), but during the 15 and 24 March, 1993.

fluctuations during the daytime. The strongest amplitudes of the GIC are linked to the strong impulses in the geoelectric field components. At LAM, $GIC = 32.0$ A at 11:00 LT on 10 January; $GIC = 27.0$ A at 12:00 LT on 20 February, 1993. Although the most important amplitudes of the
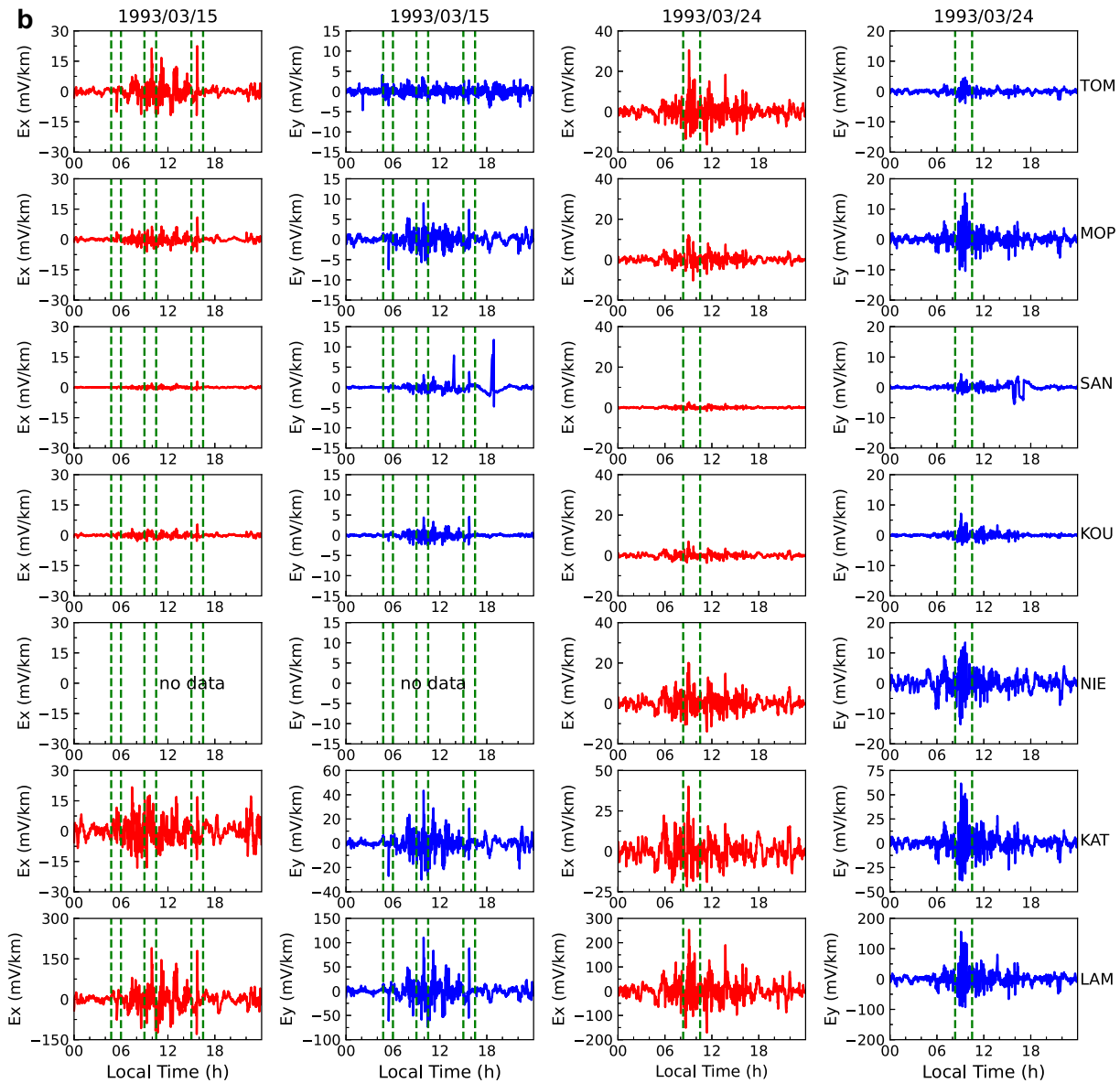
Figure 8. (*Continued.*)

GIC associated with the impulses in the geoelectric field components are observed at LAM, same impulses with weaker amplitudes are observed at the other stations of the network.

3.4.1 *Latitudinal trends of the induction effects of disturbed geomagnetic variations*

The magnitudes of Ex and Ey as well as in the GIC are relatively more important in the southern stations than in the northern stations. Figure 10 shows the latitudinal trends of the strongest impulses of the geoelectric field components Ex and Ey. The crest-to-crest amplitudes of these strongest impulses are shown in table 3. The amplitudes of the impulses decrease from LAM,

where the largest amplitudes of Ex and Ey are observed, to the weakest amplitudes at KOU and SAN. A slight increase in Ey is noticed at SIK with $Ey = 127\,\mathrm{mV/km}$, on 17 and $Ey = 51\,\mathrm{mV/km}$ on 20 February, 1993, while Ex remains relatively weak, with $Ex = 25\,\mathrm{mV/km}$ and $Ex = 8\,\mathrm{mV/km}$, respectively. At KOR and TOM, the magnitudes of the impulses in Ex slightly increase, while Ey remains decreasing.

The features of latitudinal trends of Ex and Ey are reflected in that of the GIC (figure 10). Table 4 displays the crest-to-crest amplitudes of the highest GIC impulses during the selected disturbed days. The southern stations are subject of most significant GIC amplitudes, which decrease from LAM, with slight increases at KOR, SIK and
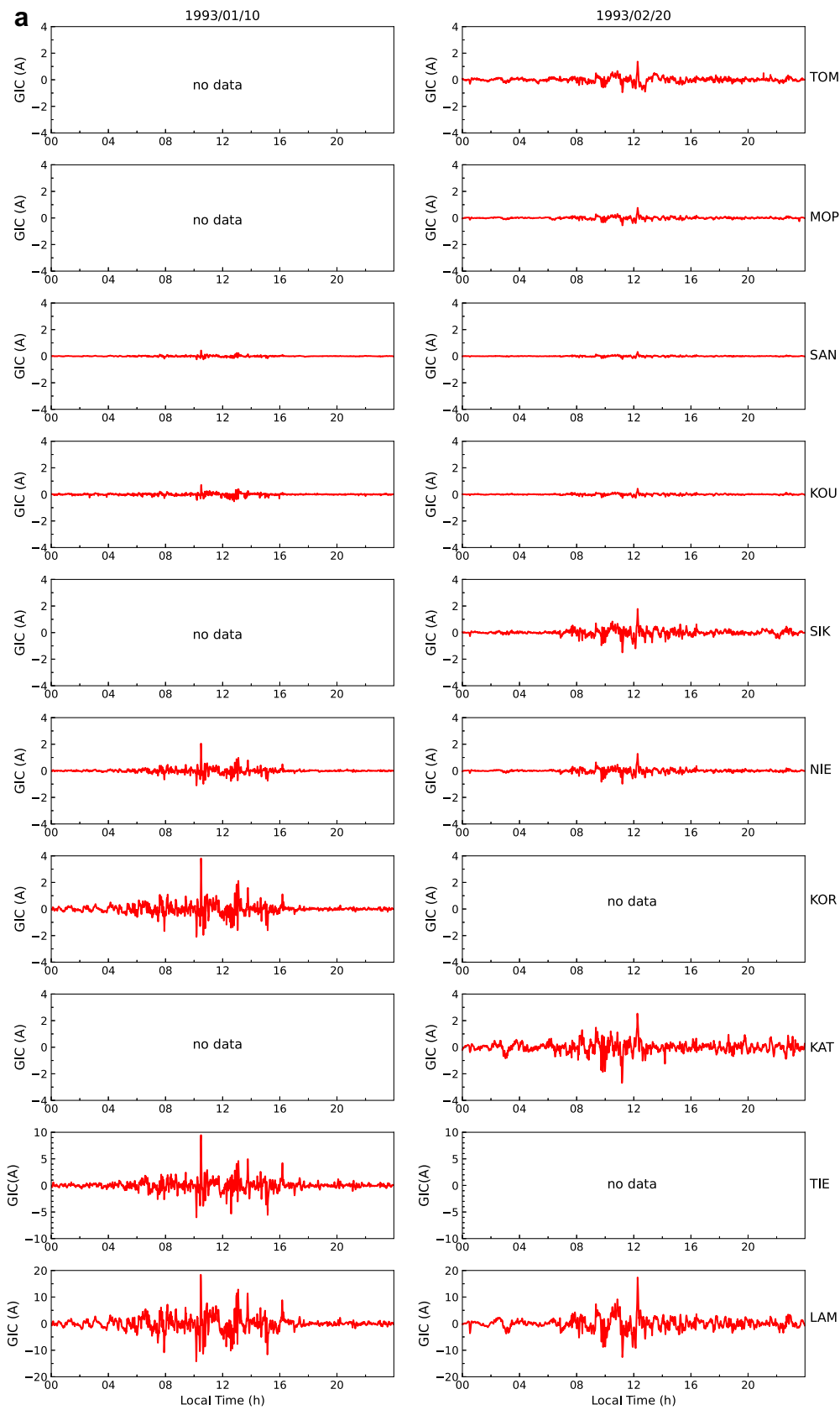
Figure 9. (**a**) Geomagnetically induced current (*GIC*) estimated from measured geoelectric field components *Ex* and *Ey* associated with geomagnetic field disturbances on 10 January and 20 February, 1993. (**b**) Same as figure 9(a), but on 15 and 24 March, 1993.
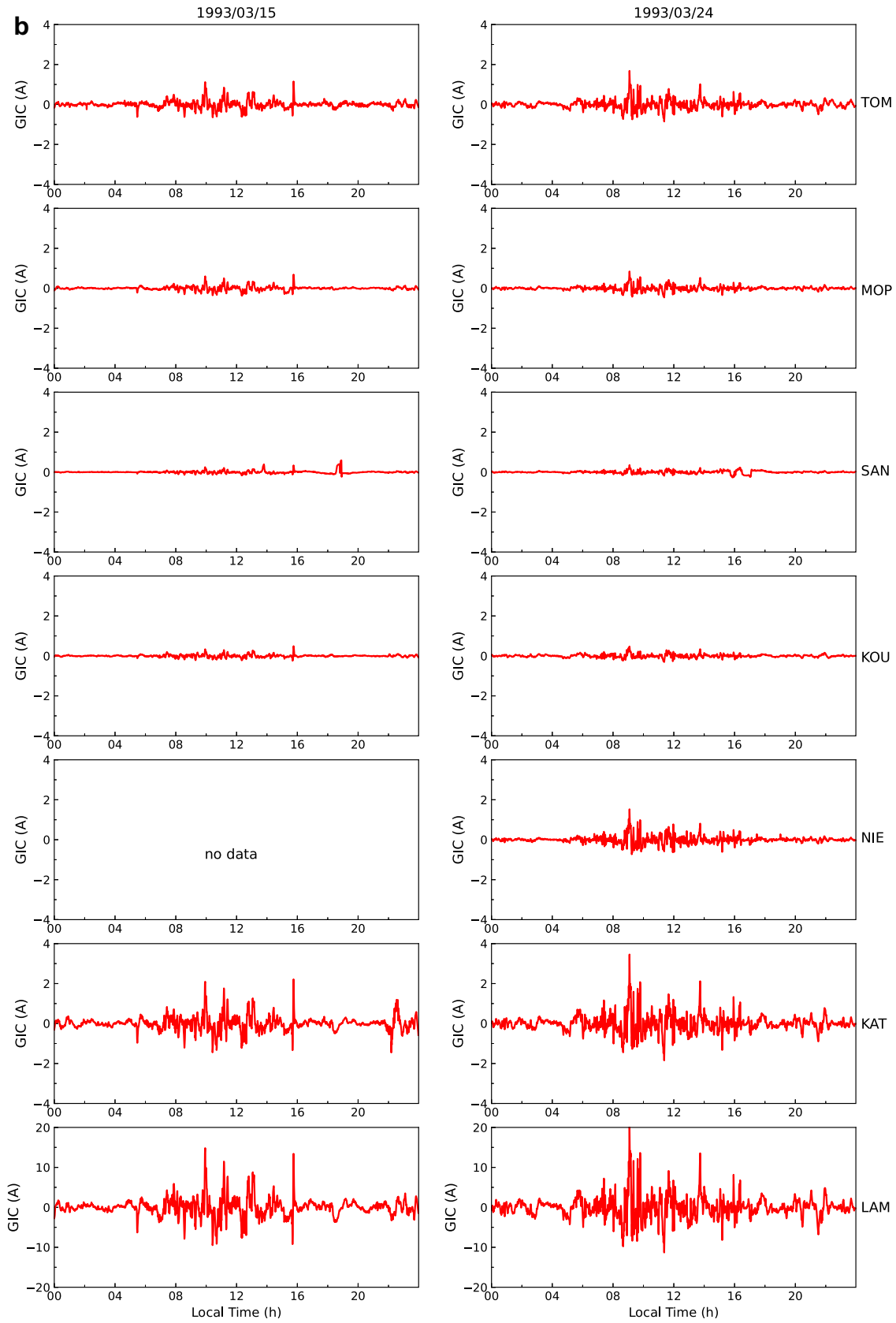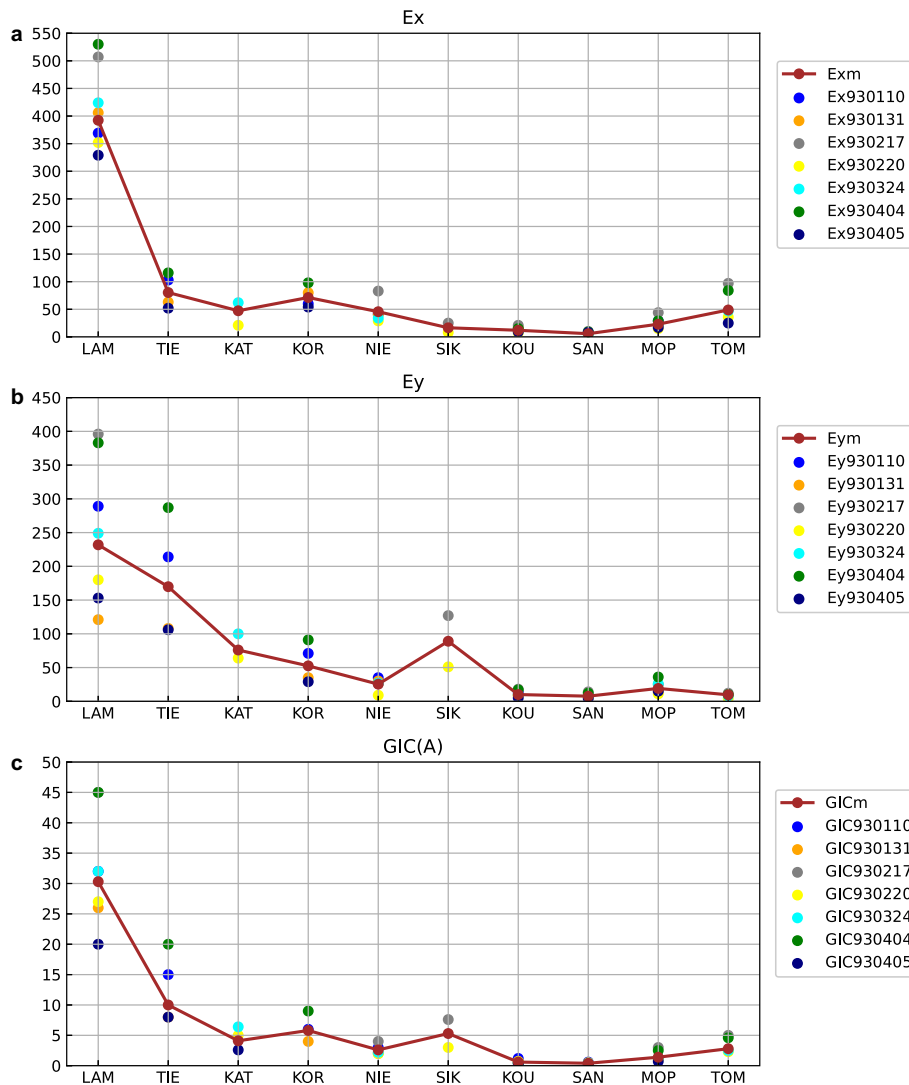
Figure 9. (*Continued.*)

Figure 10. Latitudinal trends of the impulses associated with brisk geomagnetic field variations during disturbance periods. The colored dots correspond to the impulses of individual events and the solid lines correspond to the averages of individual impulses. The geoelectric field components and the estimated *GIC* are shown: (**a**) *Ex* and *Exm*, (**b**) *Ey* and *Eym*, and (**c**) *GIC* and *GICm*.

TOM. The highest amplitudes are observed at LAM with mean $GIC = 30$ A. Non-negligible values of GIC are also observed at TIE, with mean $GIC = 10$ A. KAT and KOR experience GIC amplitudes that attain sometimes 5 A. From NIE to TOM, the GIC amplitudes are less important, with values weaker than 1 A at KOU and SAN.

4. Concluding discussion

The induction effects of disturbed geomagnetic field variations were examined through measured geoelectric field variations and associated geomagnetically induced current (GIC) in West Africa. Eleven geomagnetically disturbed days were selected with Ap index higher than 20 nT.

The geomagnetically induced current (GIC) was estimated according to equation (1), from the observed geoelectric field components Ey and Ex associated with geomagnetic disturbances based on the system parameters configuration of $a = b = 50$ A. km/V. Similar fluctuations in the time derivatives dH/dt and dD/dt of the geomagnetic field components were observed in the horizontal components Ey and Ex of the geoelectric field and the GIC variations. This similarity confirms that geoelectric field and estimated GIC fluctuations are induction effects due to geomagnetic disturbed variations. The disturbance fluctuations in the geoelectric field components and the GIC exhibit higher amplitudes during the daytime, especially between about 8:00 and 16:00 LT. These daytime amplifications are likely linked with the

Table 3. *Maximum crest to crest amplitudes of geoelectric field components during geomagnetic disturbances in West African stations. The dash indicate no data recorded.*

Stations		10/01/1993	31/01/1993	17/02/1993	20/02/1993	09/03/1993	11/03/1993	15/03/1993	16/03/1993	24/03/1993	04/04/1993	05/04/1993
						Dates						
LAM	Ex	369	406	507	352	–	–	309	305	424	530	329
	Ey	289	121	396	180	–	–	183	133	249	383	153
TIE	Ex	103	63	–	–	79	69	–	–	–	116	52
	Ey	214	108	–	–	148	156	–	–	–	287	106
KAT	Ex	–	–	–	21	71	60	40	30	62	–	–
	Ey	–	–	–	64	88	84	73	47	100	–	–
KOR	Ex	60	80	–	–	64	72	–	–	–	98	54
	Ey	71	35	–	–	46	43	–	–	–	91	29
NIE	Ex	42	40	83	29	–	–	–	–	34	–	–
	Ey	35	30	26	9	–	–	–	–	27	–	–
SIK	Ex	–	–	25	8	–	–	–	–	–	–	–
	Ey	–	–	127	51	–	–	–	–	–	–	–
KOU	Ex	15	17	21	7	10	12	8	7	11	15	9
	Ey	13	9	18	8	7	9	7	7	10	17	5
SAN	Ex	6	–	10	4	4	5	4	4	4	9	8
	Ey	8	–	14	6	5	7	4	9	7	12	4
MOP	Ex	29	22	44	15	17	24	17	17	22	29	17
	Ey	–	14	25	11	22	16	16	10	26	36	15
TOM	Ex	–	–	97	36	36	48	34	32	47	84	25
	Ey	–	–	12	4	13	15	9	6	8	10	–

Table 4. *Maximum and average GIC amplitudes estimated from geoelectric field components recorded in West African stations during the geomagnetic disturbances from January, 1993 to April, 1993. The blank boxes indicate no GIC values available because no geoelectric field data recorded in the station.*

Stations	10/01/1993	31/01/1993	17/02/1993	20/02/1993	09/03/1993	11/03/1993	15/03/1993	16/03/1993	24/03/1993	04/04/1993	05/04/1993	Averages GICm (A)
					GIC (A)							
LAM	32.0	26.0	45.0	27.0			24.0	22.0	32.0	45.0	20.0	30.3
TIE	15.0	8.0			4.0	5.0				20.0	8.0	10.0
KAT				5.0	4.3	4.0	3.6	2.6	6.4		2.6	4.1
KOR	6.0	4.0			5.0	5.0				9.0		5.8
NIE	3.0	2.0	4.0	2.0					2.2			2.6
SIK			7.6	3.0								5.3
KOU	1.2	0.7	0.5	0.7	0.6	0.4	0.7	0.2	0.5	0.4	0.4	0.6
SAN	0.6		0.3	0.5	0.4	0.2	0.8	0.5	0.4	0.3	0.3	0.4
MOP		1.2	3.0	1.0	1.0	1.3	1.0	0.7	1.2	2.5	0.7	1.4
TOM			5.0	2.3	2.0	2.5	1.7	1.6	2.5	4.6		2.8

daytime ionospheric currents, which are associated with increasing conductivity in the low latitude ionosphere (Sastry 1970; Subbaraya *et al.* 1972). Especially enhanced Cowling conductivity in the equatorial electrojet (EEJ) current belt is known to magnify geomagnetic field disturbances near the magnetic dip-equator which in turn intensifies the geoelectric field and GIC fluctuations during the daytime. The processes that underlay these effects may be analogous to ionospheric drivers of large GIC at high latitudes. Huttunen *et al.* (2002) and Pulkkinen *et al.* (2003) demonstrated the effects of

high latitude ionospheric drivers of large GIC by analyzing the GIC amplifications due to the intensifications of auroral electrojets during geomagnetic storms. The impulses in the geoelectric field components and the estimated GIC during this timeframe are stronger in the southern stations than in the northern stations. On the average, these impulses decrease from LAM to TOM, with a slight enhancement near the magnetic equator. Doumbia *et al.* (2017) attributed these important latitudinal variations to the lateral variations of the earth resistivity. Indeed, Vassal *et al.* (1998) considered two models of stratified Earth corresponding to the average resistive structure of the two tectonic provinces across the area of concern: a sedimentary basin in the north and a cratonic shield in the south. The apparent resistivity computed according to those models was found to be stronger in the cratonic shield in the south, than in the sedimentary basin in the north. The slight enhancement near the magnetic equator can also be attributed to the effect of the ionospheric conductivity at this area. In fact, Onwumechilli (1960), and Onwumechilli and Ogbuehi (1962) showed that ionospheric conductivity increases rapidly to a maximum at the EEJ dip latitude and decreases at other latitudes.

Acknowledgements

Author statement

The present work was performed in the framework of the PhD thesis of Nguessan Kouassi under the supervision of Prof Vafi Doumbia. Nguessan Kouassi and Vafi Doumbia contributed to the data processing and analysis. Vafi Doumbia verified the analytical methods and the findings of the manuscript and contributed to the discussions of the results. All the authors contributed, read and approved the final manuscript.

References

Amory-Mazaudier C, Vila P, Achache J, Achy Seka A, Albouy Y, Blanc E, Boka K, Bouvet J, Cohen Y, Dukhan M, Doumouya V, Fambitakoye O, Gendrin R, Goutelard C, Hamoudi M, Hanbaba R, Houngninou E, Huc C, Kakou K, Kobea-Toka A, Lassudrie-Duchesne P, Mbipom E, Menvielle M, Ogunade S O, Onwumechili C A, Oyinloye J A, Rees D, Richmond A, Sambou E, Schmuker E, Tirefort J L and Vassal J 1993 International equatorial electrojet year: The African sectorm; *Rev. Bras. Geofisica* **11**(**3**) 303–317.

Barbosa C, Alves L, Caraballo R, Hartmann G A, Papa A R R and Pirjola R J 2015 Analysis of geomagnetically induced currents at a low-latitude region over the solar cycles 23 and 24: Comparison between measurements and calculations; *J. Space Weather Space Clim.* **5** A35, https://doi.org/10.1051/swsc/2015036.

Bernhardi E H, Cilliers P J and Gaunt C T 2008 Improvement in the modeling of geomagnetically induced currents in southern Africa; *South Afr. J. Sci.* **104**(**7–8**) 265–272.

Bernhardi E H, Tjimbandi T A, Cilliers P J and Gaunt C T 2010 *16th Power Systems Computation Conference 2008 (PSCC 2008 Glasgow);* Glasgow, Scotland, UK, 14–18 July 2008, Presented at the Power Systems Computation Conference, Curran, Red Hook, NY. 1391–1395, ISBN 978-1-61738-857-6.

Bogdan T J 2007 Space weather: Physics and effects; In: *Space Weather: Physics and Effects* (eds) Volker Bothmer and Ioannis A Daglis, Praxis/Springer, New York, 438p, ISBN 978-3-540-23907-9; *Phys. Today* **60** 59–60, https://doi.org/10.1063/1.2825074.

Bolduc L 2002 GIC observations and studies in the Hydro-Québec power system; *J. Atmos. Sol.-Terr. Phys.* **64** 1793–1802, https://doi.org/10.1016/S1364-6826(02)00128-1.

Boteler D H 2001 Assessment of geomagnetic hazard to power systems in Canada; *Nat. Hazards* **23** 101–120, https://doi.org/10.1023/A:1011194414259.

Boteler D H, Pirjola R J and Nevanlinna H 1998 The effects of geomagnetic disturbances on electrical systems at the Earth's surface; *Adv. Space Res.* **22** 17–27, https://doi.org/10.1016/S0273-1177(97)01096-X.

de Villiers J S, Pirjola R J and Cilliers P J 2016 Estimating ionospheric currents by inversion from ground-based geomagnetic data and calculating geoelectric fields for studies of geomagnetically induced currents; *Earth Planets Space* **68** 154, https://doi.org/10.1186/s40623-016-0530-1.

Doumbia V, Boka K, Kouassi N, Grodji O D F, Amory-Mazaudier C and Menvielle M 2017 Induction effects of geomagnetic disturbances in the geo-electric field variations at low latitudes; *Ann. Geophys.* **35** 39–51, https://doi.org/10.5194/angeo-35-39-2017.

Doumouya V 1995 Etude des effets magnétiques de l'électrojet équatorial, Variabilité saisonnière et réduction des mesures magnétiques satellitaires; Thèse de Doctorat de 3e Cycle, Université Nationale de Côte d'Ivoire.

Doumouya V, Vassal J, Cohen Y, Fambitakoye O and Menville M 1998 Equatorial electrojet at African longitudes: First results from magnetic measurements; *Ann. Geophys.* **16** 658–666, https://doi.org/10.1007/s00585-998-0658-9.

Gaunt C T and Coetzee G 2007 Transformer failures in regions incorrectly considered to have low GIC-risk; In: *2007 IEEE Lausanne Power Tech.*, Switzerland, pp. 807–812, https://doi.org/10.1109/PCT.2007.4538419.

Huttunen K E J, Koskinen H E J, Pulkkinen T I, Pulkkinen A, Palmroth M, Reeves E G D and Singer H J 2002 April 2000 magnetic storm: Solar wind driver and magnetospheric response: April 2000 magnetic storm; *J. Geophys. Res. Space Phys.* **107** SMP 15-1–SMP 15-21, https://doi.org/10.1029/2001JA009154.

Kappenman J G 2003 Storm sudden commencement events and the associated geomagnetically induced current risks to ground-based systems at low-latitude and midlatitude locations: SSC events and GIC risks at low and midlatitude locations; *Space Weather* **1**, https://doi.org/10.1029/2003SW000009.

Kappenman J G 2005 An overview of the impulsive geomagnetic field disturbances and power grid impacts associated with the violent Sun-Earth connection events of 29–31 October 2003 and a comparative evaluation with other contemporary storms: Geomagnetic field disturbances and power grid; *Space Weather* **3**, https://doi.org/10.1029/2004SW000128.

Koen J 2000 Geomagnetically induced currents and their presence in the Eskom Transmission Network; MSc. (Eng) Thesis, University of Cape Town, South Africa.

Lam H L, Boteler D H and Trichtchenko L 2002 Case studies of space weather events from their launching on the Sun to their impacts on power systems on the Earth; *Ann. Geophys.* **20** 1073–1079, https://doi.org/10.5194/angeo-20-1073-2002.

Liu C M, Liu L G, Pirjola R and Wang Z Z 2009 Calculation of geomagnetically induced currents in mid- to low-latitude power grids based on the plane wave method: A preliminary case study; *Space Weather* **7**, https://doi.org/10.1029/2008SW000439.

Matandirotya E 2016 Measurement and modelling of geomagnetically induced currents (GIC) in power lines (PhD); Cape Peninsula University of Technology, South Africa, http://etd.cput.ac.za/bitstream/handle/20.500.11838/2459/210233729-MatandirotyaElectdom-Dtech-Electrical-Engineering-Eng-2017.pdf?sequence=1&isAllowed=y.

Matandirotya E, Cilliers P J and Van Zyl R R 2015 Modeling geomagnetically induced currents in the South African power transmission network using the finite element method; *Space Weather* **13** 185–195, https://doi.org/10.1002/2014SW001135.

Ngwira C M, Pulkkinen A, McKinnell L A and Cilliers P J 2008 Improved modeling of geomagnetically induced currents in the South African power network; *Space Weather* **6(11)**, https://doi.org/10.1029/2008SW000408.

Ngwira C M, Pulkkinen A A, Bernabeu E, Eichner J, Viljanen A and Crowley G 2015 Characteristics of extreme geoelectric fields and their possible causes: Localized peak enhancements; *Geophys. Res. Lett.* **42** 6916–6921, https://doi.org/10.1002/2015GL065061.

Onwumechilli A 1960 Fluctuations in the geomagnetic horizontal field near the magnetic equator; *J. Atmos.*

Terr. Phys. **17** 286–294, https://doi.org/10.1016/0021-9169(60)90141-0.

Onwumechilli A and Ogbuehi P O 1962 Fluctuations in the geomagnetic horizontal field; *J. Atmos. Terr. Phys.* **24** 173–190, https://doi.org/10.1016/0021-9169(62)90241-6.

Pirjola R 2000 Geomagnetically induced currents during magnetic storms; *IEEE Trans. Plasma Sci.* **28** 1867–1873, https://doi.org/10.1109/27.902215.

Pirjola R 2005 Effects of space weather on high-latitude ground systems; *Adv. Space Res.* **36** 2231–2240, https://doi.org/10.1016/j.asr.2003.04.074.

Pirjola R, Kauristie K, Lappalainen H, Viljanen A and Pulkkinen A 2005 Space weather risk: SPACE WEATHER RISK; *Space Weather* **3**, https://doi.org/10.1029/2004SW000112.

Pulkkinen A, Amm O and Viljanen A 2003 Ionospheric equivalent current distributions determined with the method of spherical elementary current systems: IONOSPHERIC EQUIVALENT CURRENTS; *J. Geophys. Res. Space Phys.* **108**, https://doi.org/10.1029/2001JA005085.

Pulkkinen A, Bernabeu E, Eichner J, Beggan C and Thomson A W P 2012 Generation of 100-year geomagnetically induced current scenarios: 100-year scenarios; *Space Weather* **10**, https://doi.org/10.1029/2011SW000750.

Pulkkinen A, Lindahl S, Viljanen A and Pirjola R 2005 Geomagnetic storm of 29–31 October 2003: Geomagnetically induced currents and their relation to problems in the Swedish high-voltage power transmission system: Geomagnetically induced currents; *Space Weather* **3**, https://doi.org/10.1029/2004SW000123.

Pulkkinen A, Pirjola R and Viljanen A 2007 Determination of ground conductivity and system parameters for optimal modeling of geomagnetically induced current flow in technological systems; *Earth Planets Space* **59** 999–1006, https://doi.org/10.1186/BF03352040.

Sastry T S G 1970 Diurnal changes in the parameters of the equatorial electrojet as observed by rocket-borne magnetometers; *Space Res.* **10** 778–785.

Subbaraya B H, Muralikrishna P, Sastry T S G and Prakash S 1972 A study of the structure of electrical conductivities and the electrostatic field within the equatorial electrojet; *Planet. Space Sci.* **20** 47–52, https://doi.org/10.1016/0032-0633(72)90139-0.

Torta J M, Serrano L, Regué J R, Sánchez A M and Roldán E 2012 Geomagnetically induced currents in a power grid of northeastern Spain: GICs in a Spanish power grid; *Space Weather* **10**, https://doi.org/10.1029/2012SW000793.

Trivedi N B, Vitorello Í, Kabata W, Dutra S L G, Padilha A L, Bologna M S, de Pádua M B, Soares A P, Luz G S, Pinto F de A, Pirjola R and Viljanen A 2007 Geomagnetically induced currents in an electric power transmission system at low latitudes in Brazil – A case study: GIC in Brazilian electric power system; *Space Weather* **5**, https://doi.org/10.1029/2006SW000282.

Vassal J, Menvielle M, Cohen Y, Dukhan M, Doumouya V, Boka K and Fambitakoye O 1998 A study of transient variations in the Earth's electromagnetic field at equatorial electrojet latitudes in western Africa (Mali and the Ivory Coast); *Ann. Geophys.* **16** 677–697, https://doi.org/10.1007/s00585-998-0677-6.

Viljanen A and Pirjola R 1994 Geomagnetically induced currents in the Finnish high-voltage power system: A

geophysical review; *Surv. Geophys.* **15** 383–408, https://doi.org/10.1007/BF00665999.

Wik M, Pirjola R, Lundstedt H, Viljanen A, Wintoft P and Pulkkinen A 2009 Space weather events in July 1982 and October 2003 and the effects of geomagnetically induced currents on Swedish technical systems; *Ann. Geophys.* **27** 1775–1787, https://doi.org/10.5194/angeo-27-1775-2009.

Zois I P 2013 Solar activity and transformer failures in the Greek national electric grid; *J. Space Weather Space Clim.* **3** A32, https://doi.org/10.1051/swsc/2013055.

Corresponding editor: T Narayana Rao